Amyloidogenic Peptide/Single-Walled Carbon Nanotube Composites Based on Tau-Protein-Related Peptides Derived from AcPHF6: Preparation and Dispersive Properties

ARTICLE *in* THE JOURNAL OF PHYSICAL CHEMISTRY B · JUNE 2013

Impact Factor: 3.3 · DOI: 10.1021/jp402057d · Source: PubMed

5 AUTHORS, INCLUDING:

Anju Sreelatha
University of Texas Southwestern Medical Cen…
7 PUBLICATIONS **88** CITATIONS
SEE PROFILE

Warren Goux
University of Texas at Dallas
64 PUBLICATIONS **1,583** CITATIONS
SEE PROFILE

THE JOURNAL OF PHYSICAL CHEMISTRY B

Article

pubs.acs.org/JPCB

Amyloidogenic Peptide/Single-Walled Carbon Nanotube Composites Based on Tau-Protein-Related Peptides Derived from AcPHF6: Preparation and Dispersive Properties

Edgar Muñoz,*[,†] Anju Sreelatha,[‡] Rosa Garriga,[§] Ray H. Baughman,[⊥,#] and Warren J. Goux*[,⊥]

[†]Instituto de Carboquímica ICB-CSIC, Miguel Luesma Castán 4, 50018 Zaragoza, Spain

[‡]Department of Molecular Biology, The University of Texas Southwestern Medical Center, Dallas, Texas 75390, United States

[§]Departamento de Química Física, Universidad de Zaragoza, 50009 Zaragoza, Spain

[⊥]Department of Chemistry and [#]The Alan G. MacDiarmid NanoTech Institute, The University of Texas at Dallas, Richardson, Texas 75080, United States

Supporting Information

ABSTRACT: We investigated the abilities of a family of tau-protein-related amphiphilic peptides with predictable self-association characteristics (*N*-acetyl-VQIVXK-NH_2 (X = F, L, V, W, Y, A, K)) to disperse single-walled carbon nanotubes (SWCNTs). The dispersion abilities of these peptides could be explained by a linear combination of their hydrophobic and amyloidogenic properties in a 60/40 ratio. Circular dichroism (CD) spectra of one of the peptides having a high propensity to form an amyloid (*N*-acetyl-VQIVYK-NH_2 (AcPHF6)) showed that this peptide exists as a random coil in water but assumes a β-sheet conformation when sonicated with SWCNTs. Electron microscopy results, changes in near-infrared spectra, and changes in the Raman spectra upon formation of composites suggest that AcPHF6 intercalates, coats, and exfoliates SWCNT bundles. N-terminal truncation of AcPHF6 greatly reduced its ability to disperse SWCNTs. Taken together, our results suggest that amyloidogenic peptides wrap SWCNTs, forming an extensive β-sheet network. To date, peptides based on the AcVQIVXK framework are structurally the simplest peptides that have been found to disperse CNTs, and an understanding of those properties that determine their efficiency may be used to design even more efficient peptides for these purposes. We believe that due to the structural simplicity, this family of peptides will have clear synthetic advantages over peptides now known to disperse CNTs.

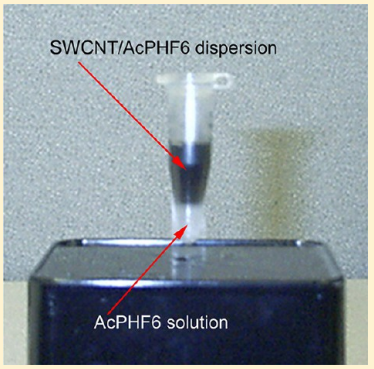

1. INTRODUCTION

The preparation of carbon nanotube (CNT)-based biohybrids with peptides enables CNT dispersion in aqueous media and may eventually facilitate their incorporation into biological systems,[1−6] biosensors, drug delivery systems, and other biomedical and biotherapeutic applications.[7−13] In the past, amphiphilic α-helical peptides, having one face of the helix with hydrophobic residues and the other face with charged or polar residues, have been designed to disperse single-walled carbon nanotubes (SWCNTs).[1,5,14−16] Other nonhelical amphiphilic peptides that possess hydrophobic pockets have been mined from phage display libraries or protein digests to yield optimal peptide/SWCNT dispersions.[18−27] In the majority of cases, these peptides either assume a β-sheet conformation, forming amyloid filaments by self-assembly,[25−27] or are random coil and transition to β-sheet or β-hairpin structures on the surface of the carbon nanoparticle.[17,18,20,22−24,28]

The ability of a peptide to disperse carbon nanostructures appears to depend upon its binding affinity to the sp^2-hybridized surface of the SWCNTs and its amphiphilic or detergent-like properties. Although it has been found that aromatic residues have an enhanced affinity for the hydrophobic surface of the carbon nanoparticle by virtue of $\pi-\pi$ stacking forces,[1,14−19,23,24,28−33] it has also been shown that some amphiphilic peptides containing aliphatic side chains in place of aromatic side chains are also able to very efficiently disperse SWCNTs.[26,27] For example, poly-L-lysine has been shown to disperse SWCNTs, either by virtue of the C_4H_8 moiety contained in its side chain interacting with the nanotube surface by van der Waals forces or by cation$-\pi$ attractive interactions between the positive charged primary amino group and the SWCNT surface.[24,26,31,34−36] In addition, it has been shown that charge transfer between aromatic side chains or amines and SWCNT surfaces may also be important in noncovalent interactions.[15,30,37,38] While all of these attractive interactions are clearly important in the ability of peptides to bind to CNTs, the amphiphilic nature of the peptide sequence allows the peptide to disperse CNTs in an aqueous environment.

Received: February 27, 2013
Revised: May 2, 2013
Published: June 7, 2013

   dx.doi.org/10.1021/jp402057d | *J. Phys. Chem. B* 2013, 117, 7593−7604

The dispersive ability of biomacromolecules may also depend on their ability to form organized structures on the nanotube surface. RNAs, single- and double-strand DNAs,[39−41] polysaccharides,[42,43] and cyclic peptides[21,44] have been shown to bind to SWCNTs by wrapping around tubes in an organized fashion, and in some cases, biopolymer/CNT complexes have served as a basis of tube sorting. Recently, it has been shown that peptides with structures containing alternate hydrophobic and hydrophilic residues form organized β-sheet structures on the surface of SWCNTs, and the composites formed lead to enhanced optical and physicochemical properties for selected tube types.[24−27] These results agree with molecular mechanics and dynamics simulations showing β-sheets that can assemble into β-barrels wrapping the SWCNTs.[24,45] Because some of these peptides fail to form β-sheet structures in the absence of SWCNTs, it has been suggested that the SWCNT surface acts as a template for peptide self-assembly.[26,45] While it has been experimentally shown that the propensity to form amyloid or coat SWCNT surfaces depends on the peptide composition, sequence, and length,[24,26] so far, a detailed understanding of specific interactions leading to the ability of a peptide to uniformly coat SWCNTs and its dependence on peptide structure has remained elusive.

Over the past several years, our laboratory has been studying a family of hexapeptides, *N*-acetyl-VQIVXK-NH_2 (X = any amino acid residue other than cysteine), derived from tau protein and their ability to seed self-assembly of the protein into paired helical filaments (PHFs) associated with Alzheimer's disease.[46−50] In pure water, only a small fraction of these peptides form amyloid, but in the presence of even low concentrations of added salt or buffer, we have been able to derive an amyloidogenic propensity scale based on the amino acid residue substituted in the penultimate position of the sequence.[48] In this investigation, we use these peptides, as well as N-terminally truncated versions of the peptide *N*-acetyl-VQIVYK-NH_2 (AcPHF6), to study the effect that hydrophobicity, sequence length, and amyloidogenic propensity have on the ability to disperse SWCNTs.

2. EXPERIMENTAL METHODS

2.1. Materials. SWCNTs produced by high-pressure decomposition of carbon monoxide (HiPco process)[51] were purchased from Carbon Nanotechnologies Inc. (batch # R0210). Purified SWCNTs produced by the pulsed laser vaporization method (PLV)[52] were purchased from Tubes@Rice (lot # PO42600s21). SWCNTs produced using the PLV method have an average diameter of approximately 1.3 nm. Elemental analysis data revealed that this SWCNT material was 84.43% C, 1.26% H, 0.20% N, 9.61% O, 1.4% Ni, and 1.49% Co. HiPco SWCNTs have a diameter distribution between 0.7 and 1.2 nm. Carbon Nanotechnologies HiPco SWCNTs were 61.05% C and 37.98% Fe.

AcPHF6 was purchased from Macromolecular Resources (Fort Collins, CO). All other peptides were prepared by solid-phase peptide synthetic methods according to previously published procedures and purified by reverse-phase HPLC using a water−acetonitrile gradient.[48] The purity was checked using ESI-MS or MALDI-TOF MS.

2.2. HPLC Retention Times. Retention times for all peptides were determined on a 250 × 4.6 mm C18 column (Alltech Adsorbosil, Nicholasville, KY) using a linear gradient (0−100%) of water and acetonitrile (each containing 0.1% TFA) over 30 min at a flow rate 1 mL/min and were used as a measure of peptide hydrophobicity.[48]

2.3. Preparation of AcPHF6/SWCNT Composites. AcPHF6 stock solutions were prepared in water at 1 mg/mL, and concentrations were measured by absorbance using published molar extinction coefficients.[46,48] For preparation of AcPHF6/SWCNT composites used for Raman, CD, and microscopy studies, peptide stock solutions were probe-sonicated with 1 mg of SWCNTs. Sonication was carried out on ice for 1 min with a Sonics & Materials, Inc. (Newton, CT) model VC-50 Vibra Cell sonicator equipped with a 4 mm diameter microtip using a power level of 12−15 W. Over time, this resulted in a biphasic solution with a AcPHF6/SWCNTs composite on the top and water/AcPHF6 on the bottom. Stock solutions were prepared by centrifugation of the top composite layer at 6000 g (14 000 rpm) for 10 min. These solutions were used for TEM and Raman analysis.

2.4. UV−Vis−Near-Infrared (NIR) Studies. For NIR studies, peptide stock solutions varying in concentration from 0.01 to 1.0 mM were sonicated with 1 mg of HiPco SWCNTs (Unidyn) using a Misonix Sonicator 3000 ultrasonic liquid processor equipped with a 3.2 mm probe tip. Solutions were sonicated on ice for 3 min at a power setting of 3 W. The solutions were then centrifuged at 16 000 g (14 000 rpm) for 10 min. Approximately 850 μL of supernatant was removed and ultracentrifuged at 87 450 g (46 000 rpm) for 30 min. Approximately 800 μL of supernatant was transferred into a clean vial and used for spectroscopy. The amount of SWCNTs in solution was estimated from the absorbance band at 735 nm (8,7).[21,39] Spectra were acquired on a Shimadzu UV-1700 spectrophotometer. Absorbances were correlated to the amyloidogenic propensity[48] and HPLC retention time (used as a measure of hydrophobicity) using regression analysis involving two independent variables. All variable were independently scaled to unit variance.

2.5. CD Measurements. CD measurements were carried out on AcPHF6/SWCNT composites in water and AcPHF6 in water or 20 mM 3-(*N*-morpholino)propanesulfonic acid, adjusted to pH 7.0 (MOPS buffer) using an Aviv model 202 circular dichroism spectrometer. Spectra were collected with a 0.2 mm circular quartz cuvette at 1 nm intervals. Each spectrum was an average of four or eight scans with a signal averaging time of 2 s at each wavelength. After subtracting a blank, spectra were smoothed using five data point block averaging and converted to the mean residue ellipticity using concentrations determined from the UV absorbance.

2.6. Raman Measurements. Raman spectra were collected with a Jobin-Yvon Horiba high-resolution LabRam Raman microscope system (helium−neon laser operating at 35 nW, λ_{exc} = 632.8 nm; transition energy: 1.96 eV). Spectra were recorded by scanning the 50−3000 cm^{-1} region with a total acquisition time of 8 min. The power of the laser spot (~1 μm in diameter) focused on the sample was ~8 mW. Wavenumber calibration was carried out using the 520.5 cm^{-1} line for a silicon wafer. A spectral resolution of ~1 cm^{-1} was used.

2.7. Electron Microscopy Characterization. AcPHF6/SWCNT dispersions were freeze-dried, deposited on conducting carbon tape, and then gold coated (~5 μm thick) for scanning electron microscopy (SEM) characterization (LEO 1530 VP microscope; accelerating voltage: 10−15 kV). Samples for TEM were typically prepared by diluting AcPHF6/SWCNT stock solutions 1:10 or 1:100 with water and placing a 10 μL drop of the diluted sample onto a 200 mesh Formvar carbon-

dx.doi.org/10.1021/jp402057d | J. Phys. Chem. B 2013, 117, 7593−7604

coated copper grid and allowing the solvent to evaporate at room temperature. TEM characterization was performed with a JEOL 1200EX microscope (accelerating voltage: 80 kV).

3. RESULTS

The peptide VQIVYK is a homologous sequence from tau protein, a microtubule-associated protein that aggregates to produce neurofibrillary tangles (NFTs) in neurons of patients with Alzheimer's disease and other tauopathies.[46−50,53,54] In buffer at neutral pH, the blocked peptide analogue, AcPHF6, rapidly aggregates into amyloid fibrils in which the peptide assumes antiparallel layers of parallel in-register β-sheet peptide (Figure 1).[47,50,55] In water, AcPHF6 remains predominantly

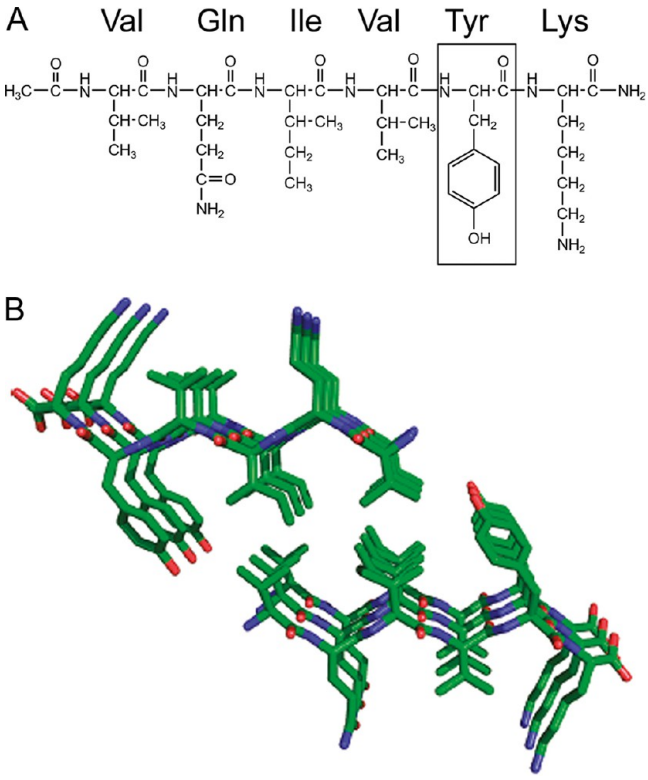

Figure 1. Structure of AcPHF6 (A). (B) X-ray structural determination suggests that peptide chains pack in antiparallel layered, parallel in-register peptide chains.

monomeric, with only a small fraction of the sample in the filamentous state.[46,48] In our previous studies, we found that the driving force for β-sheet formation was the physical characteristics of the amino acid residues and their sequence in the peptide.[48] We have likened the sequence of AcPHF6 to that of a "peptide detergent" with a sequence of mostly hydrophobic amino acids starting at the N-terminus and a charged lysine at the C-terminus.[48,49] We hypothesized that these properties would allow the hydrophobic tail of the peptide to interact with the SWCNT surface and the C-terminal charged lysine to pull the SWCNTs into solution. In order to help us further evaluate the importance that β-sheet structures have on the ability of peptides to disperse SWCNTs, we chose to investigate a family of AcPHF6 derivatives in which the penultimate residue in the sequence is substituted for one of six other amino acids that vary in side chain charge and hydrophobicity. We have previously shown that these peptides vary in their ability to form amyloid structures in buffered solution, and we have used a bevy of physical measurements to derive "amyloidogenic propensities".[48] The structures of these peptides and their amyloidogenic propensities along with other N-terminal truncated peptides used in this study are summarized in Table 1. On the basis of the propensity scale shown in the table,

Table 1. Peptides Used in This Study

peptide	sequence	amyloidogenic propensity[a]
AcPHF6	Ac-VQIVYK-NH_2	4.59
PHF6	H_2N-VQIVYK-CO_2H	
AcVQIVFK	Ac-VQIVFK-NH_2	2.80
AcVQIVWK	Ac-VQIVWK-NH_2	2.20
AcVQIVLK	Ac-VQIVLK-NH_2	1.70
AcVQIVAK	Ac-VQIVAK-NH_2	0.52
AcVQIVVK	Ac-VQIVVK-NH_2	2.54
AcVQIVKK	Ac-VQIVKK-NH_2	−3.67
AcPHF5	Ac-QIVYK-NH_2	
AcVVK	Ac-VYK-NH_2	
AcYK	Ac-YK-NH_2	

[a]Amyloidogenic propensity of the penultimate amino acid taken from ref 48.

the peptides are likely to form amyloid in the order AcPHF6 > AcVQIVFK > AcVQIVVK > AcVQIVWK > AcVQIVLK. The peptides with the lowest propensity values, AcVQIVAK and AcVQIVKK, do not form appreciable amyloid even in buffered solution.[48]

We first characterized composites of AcPHF6 with SWCNTs. Probe sonication of 1.2 mM AcPHF6 in water with HiPco SWCNTs formed a biphasic solution with an AcPHF6/SWCNT composite on the top layer and an AcPHF6 solution on the bottom layer (Figure 2). We found this solution

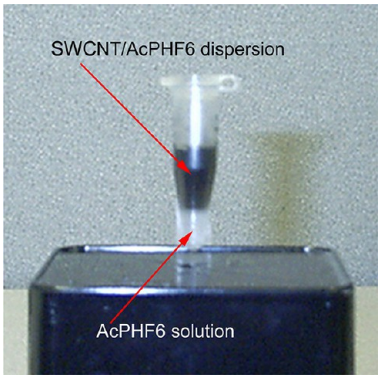

Figure 2. SWCNT/AcPHF6 mixtures form a stable composite in water following probe sonication. Following aging, a biphasic system is observed with the composite as the top layer and AcPHF6 solution in the lower layer.

to be stable for at least 1 year. Similar results were obtained for AcPHF6/PLV SWCNT composites. TEM micrographs of AcPHF6 fibers and AcPHF6/SWCNT composites are shown at low and high resolution in Figure 3. AcPHF6 filaments were composed of two parallel protofilaments, 5 ± 1 nm in width and 1−2 μm in length (Figure 3A and B). AcPHF6 filaments were also visible in the low-resolution image for the HiPco AcPHF6/SWCNT composite, where they are seen intertwined with HiPco CNT bundles (identifiable by high-contrast Fe catalysts associated with the SWCNT, which acts as a natural "stain") (Figure 3C). At high resolution, the HiPco SWCNT

dx.doi.org/10.1021/jp402057d | J. Phys. Chem. B 2013, 117, 7593−7604

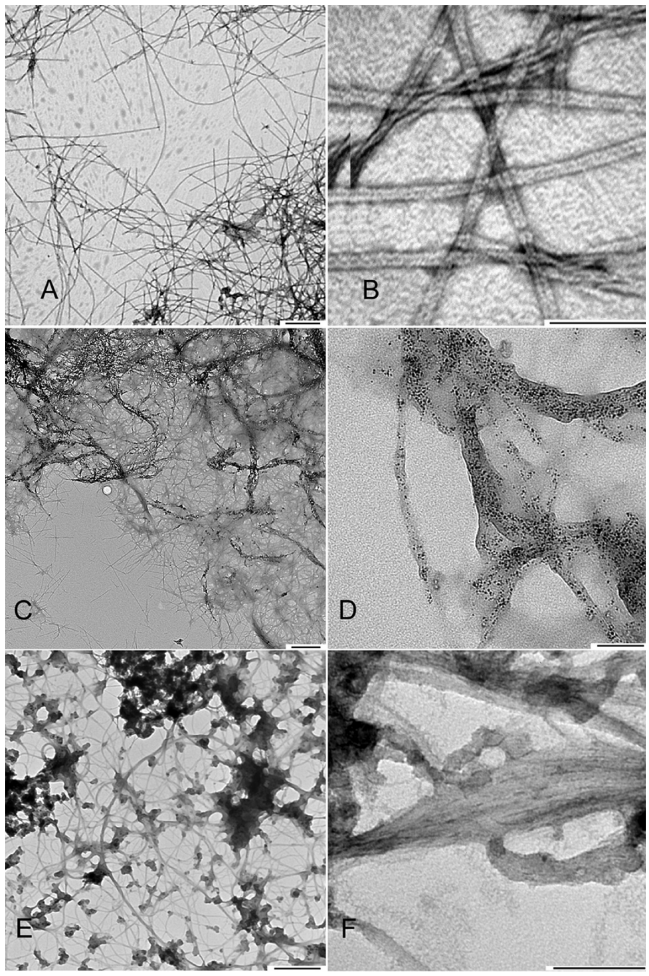

Figure 3. TEM micrographs of AcPHF6 (A,B), the AcPHF6 (1 mg/mL)/HiPco SWCNT (1 mg/mL) composite (C,D), and the AcPHF6 (1 mg/mL)/PLV SWCNT (1 mg/mL) composite (E,F). Scale bars are 500 (A, C, E) or 100 nm (B, D, F).

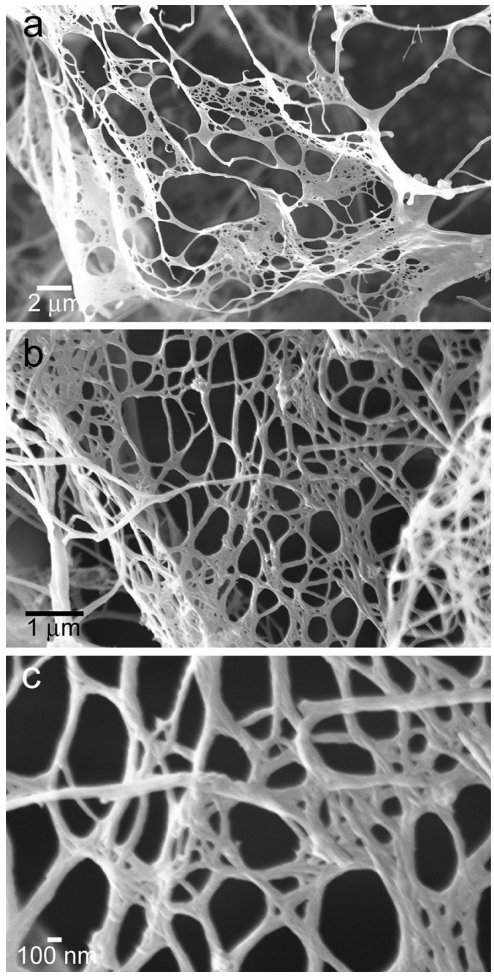

Figure 4. SEM micrographs of AcPHF6/HiPco SWCNT (A) and PHF6/PLV SWCNT (B) freeze-dried composites. A higher-resolution SEM image of the reticular structure of these assemblies is depicted in (C).

bundles are seen covered on their outer walls with a diffuse amorphous coating (Figure 3D). It is more difficult to distinguish PLV SWCNT bundles from AcPHF6 filaments by TEM (Figure 3E and F). The Ni−Co catalysts used in PLV SWCNT synthesis[52] (which are embedded within amorphous carbon) could be identified in these AcPHF6/SWCNT composites, where the peptide appeared to form a film over the SWCNT bundles (top left of Figure 3E and F). Our results indicate that this AcPHF6 coating on the SWCNT bundles accounts for the efficient dispersion of SWCNTs in water. Singular, unique reticular structures can be achieved by freeze-drying AcPHF6/SWCNT for both PLV and HiPco composites (Figure 4A and B, respectively). Higher-resolution SEM images (Figure 4C) also suggest that there is a strong interaction between fibrillar structures (peptide and SWCNTs) within the composites.

Resonance Raman spectroscopy has been shown to be a valuable method for determining the nature of the interactions between SWCNTs and bio- or organic polymers, where peaks appearing in the spectrum correspond to different tube types in resonance with a given laser excitation wavelength.[56] In general, two features dominate the spectrum of SWCNTs, a low-frequency radial breathing mode (RBM; 100−400 cm^{-1}) and a high-frequency tangential mode (TM or G band; 1500−1600 cm^{-1}). The RBM frequencies ω_{RBM} are diameter-dependent according to the empirical relationship[56−59]

$$\omega_{RBM} = \frac{c_1}{d_t} + c_2 = \frac{\pi c_1}{a_{c-c}\sqrt{3(n^2 + nm + m^2)}} + c_2 \quad (1)$$

where c_1 = 223.5 cm^{-1} and c_2 = 12.5 cm^{-1}, a_{c-c} = 0.144 nm, and d_t is the nanotube diameter (nm). Using this expression, given tube types (n,m) may be assigned to RBM frequencies. According to empirical data for the dependence of van Hove resonant transition energies on tube diameter (Kataura plot), metallic tubes from 1.0 to 1.4 nm and semiconducting tubes from 0.6 to 1.0 nm are expected to be in resonance with the 633 nm (1.96 eV) laser excitation used in our study.[56] The resonance Raman spectrum of pristine HiPco SWCNT powder shows a number of RBM peaks that result from a heterogeneity of nanotube types in the sample (Figure 5A). Peaks at 192, 203, and 216 cm^{-1} have previously been assigned to larger diameter metallic tubes (12,6), (9,9), and (13,4) (predicted ω_{RBM} = 189.8, 193.1, and 196.4 cm^{-1}), (10,7) (predicted ω_{RBM} = 202.7 cm^{-1}), and (12,3) (predicted ω_{RBM} = 217.3 cm^{-1}), while peaks at 243 and 256 cm^{-1} can be assigned to smaller diameter metallic and semiconducting tubes (11,2) and (11,1) (predicted ω_{RBM} = 244.7 and 256.6 cm^{-1}).[57−61] The tangential mode (G band) is split into a higher-frequency G^+ band

dx.doi.org/10.1021/jp402057d | J. Phys. Chem. B 2013, 117, 7593−7604

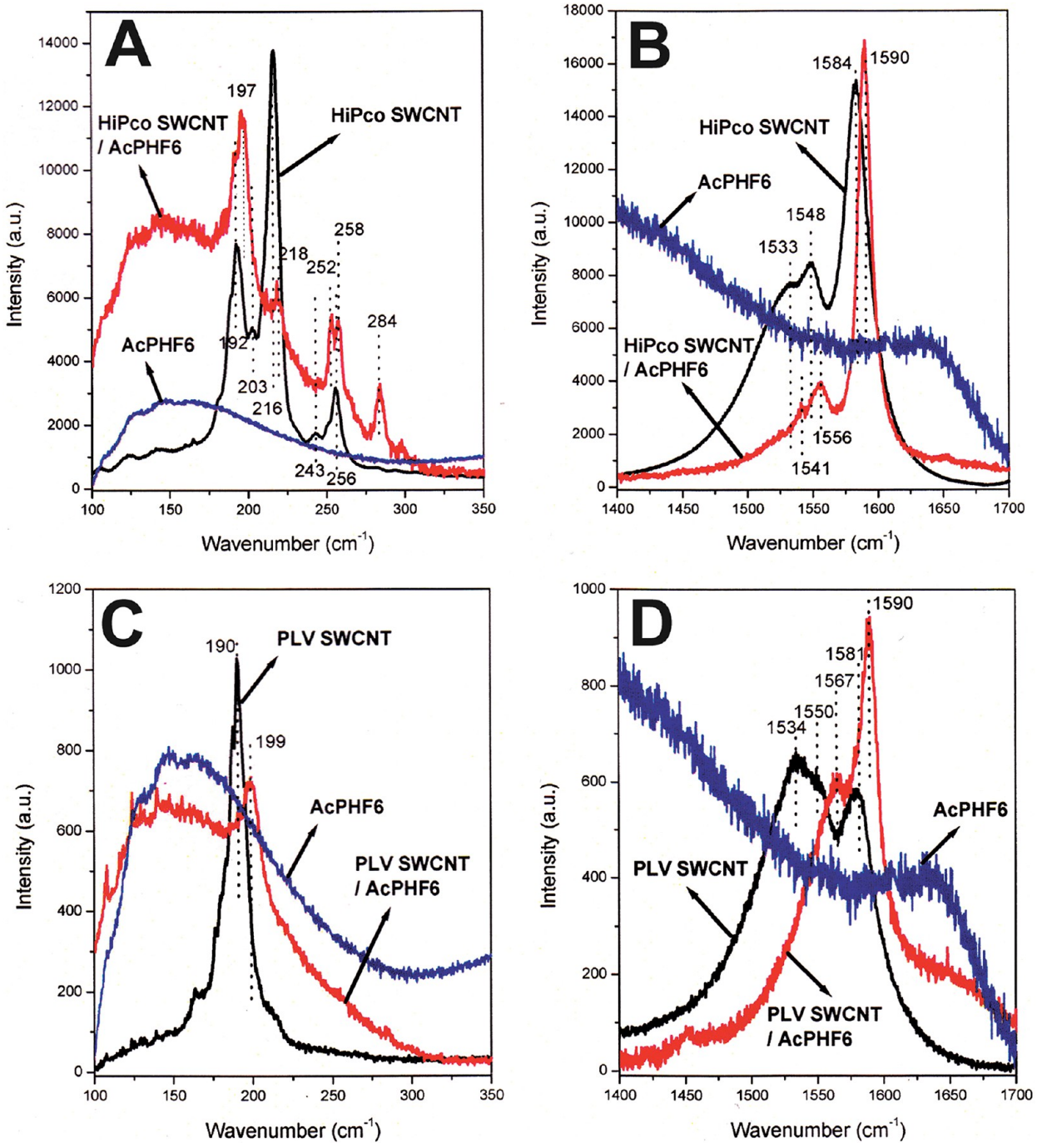

Figure 5. Raman RBM and TM (G band) of HiPco (A,B) and PLV (C,D) SWCNTs and their AcPHF6 composites.

corresponding to a diameter-independent longitudinal component for atomic displacement along the tube axis and a lower-frequency G^- band corresponding to a diameter-dependent transverse component for modes with atomic displacement along the circumferential direction. Splitting between these two component bands increases as $1/d_t^2$, such that the larger diameter metallic tubes in the G^- band lie at lower frequencies than smaller diameter semiconducting tubes.[56,61] The G band in the Raman spectrum of HiPco SWCNTs is shown in Figure 5B. On the basis of previous work, the sharper, more intense band at 1584 cm^{-1} can be assigned to the G^+ band arising from both metallic and semiconducting tubes, while the broad G^- band between 1500 and 1560 cm^{-1} has been fit to higher-frequency Lorentzian components arising from semiconducting tubes and lower-frequency Lorentzian and Breit−Wigner−Fano (BWF) components arising from metallic tubes.[56,62−64] The asymmetric BWF line shape of the metallic G^- band accounts for its trailing at lower frequencies (<1500 cm^{-1}). There are no discernible peaks in the Raman associated with AcPHF6, although there appears to be a broad background from the peptide in the RBM region of the AcPHF6/HiPco SWCNT composite spectrum (Figure 5A). We compare the Raman on pristine HiPco powder to that of the AcPHF6/HiPco SWCNT composite following centrifugation at 6000 g. Centrifugation at this speed removes larger composite bundles but does not in general yield individual peptide-coated SWCNTs. Nevertheless,

dx.doi.org/10.1021/jp402057d | J. Phys. Chem. B 2013, 117, 7593−7604

changes in the Raman spectrum of SWCNTs composites with polymers, detergents, peptides, and DNAs have demonstrated the effects of debundling.[1,29,44,61,65−67] In general, bundling perturbs the electronic and vibrational properties of single tubes, bringing some tubes into or out of resonance with the laser excitation frequency. Changes due to debundling have been observed in both the RBM and the G regions and have been seen using laser excitation wavelengths of 488,[44] 633,[1,15,29,30,44,61,66] 785,[65] and 1064 nm.[67−69] In the RBM region of the AcPHF6/HiPco SWCNT Raman using a 633 nm excitation, the superposition of metallic bands at 192 cm^{-1} is upshifted by 5 cm^{-1}, while the metallic band at 216 cm^{-1} (13,4) is upshifted by 2 cm^{-1} and much decreased in intensity. The absence of the (13,4) band near 218 cm^{-1} has previously been used as an indicator for debundling.[61] New bands appear at 252 and 284 cm^{-1} in the composite sample, which likely can be assigned to semiconducting tubes (10,3) (predicted ω_{RBM} = 251.3 cm^{-1}) and (7,5) (predicted ω_{RBM} = 282.1 cm^{-1}), and the 256 cm^{-1} (11,1) band is upshifted by 2 cm^{-1}. The appearance or augmentation of the band near 284 cm^{-1} has previously been observed for SWCNT composites with peptides[1,44] and for SDS/HiPco SWCNT composites[61] and has been used in the assessment of tube debundling.[44] The metallic band at 243 cm^{-1} (11,2), which appeared just above the noise level in the Raman of pristine HiPco SWCNTs, is not detected in the spectrum of the AcPHF6/HiPco SWCNT composite. These observed changes in the RBM features of the composite when compared to those of the pristine SWCNTs are commonly assigned to strong peptide/peptide interfacial interactions with SWCNTs that lead to efficient peptide/polymer intercalation within SWCNT bundles[1,66,67] Figure 5B shows that the G^- band is reduced in intensity, and the absence of the BWF line width is associated with metallic tube types, while the G^+ band becomes narrower and is upshifted by 6 cm^{-1}. Similar changes in the G bands have been attributed to tube debundling in HiPco SWCNT composites with peptides,[1] detergents,[61] and polymers,[66] and these have been attributed to debundling or to charge-transfer interactions.[15,30,67,70] The RBM region of the PLV SWCNT Raman (Figure 5C) shows only the 190 cm^{-1} band previously assigned to metallic tubes, and this band is upshifted and of decreased intensity in the AcPHF6/PLV SWCNT Raman. There is an upshift in the G^- band of the composite sample (Figure 5D), largely due to the absence of the contribution that metallic tubes make to the BWF line width, while the G^+ band is upshifted by 9 cm^{-1} and is decreased in line width. These changes are consistent with those seen for detergent,[61,68,69] DNA[62] and peptide/PLV SWCNT composites[1] and, as was the case for the AcPHF6/HiPco SWCNT composites, have been attributed to tube debundling. In summary, our Raman results suggest that AcPHF6 coats and exfoliates HiPco and PLV SWCNTs.

Figure 6 shows the far-UV CD spectrum of AcPHF6 in water and the same peptide following the addition of HiPco SWCNTs to form a stable composite. The CD spectrum of the peptide in water displays a negative band between 195 and 200 nm and a weak negative shoulder near 220 nm, typical of proteins with a high fraction of random coil or polyproline II structure.[48,71] This spectrum is consistent with our previous findings showing that the peptide in water is primarily monomeric and contains only a minor fraction of amyloid.[46,48] In marked contrast to the CD spectrum of AcPHF6 in water, the CD spectrum of the peptide/HiPco composite displays a negative band near 218 nm and a positive band between 190

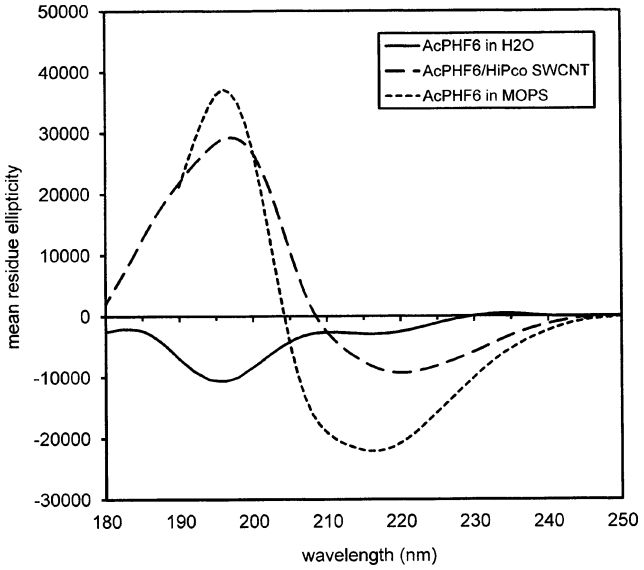

Figure 6. CD spectra of AcPHF6 (1 mg/mL) in water or MOPS buffer and an AcPHF6 (1 mg/mL)/HiPco SWCNT (1 mg/mL) composite (in water) after 4 weeks of aging at room temperature.

and 200 nm, typical of peptides having a high fraction of extended β-sheet structure. Because commonly used fitting routines for estimating secondary structure from CD data cannot be used for short peptides where the contribution from aromatic residues could be significant,[72,73] the relative fraction of β-sheet structure was not determined. Irrespective of this limitation, our results suggest that the fraction of β-sheet structure is significantly greater for the peptide in the presence of the SWCNTs as a result of the binding of the AcPHF6 to the SWCNT surface. Similar conformational changes from a random coil to β-sheet have been observed in other peptides optimized to form composites with SWCNTs and multiwalled carbon nanotubes (MWCNTs).[16−18,21−23] For comparison, the CD spectrum of AcPHF6 in MOPS buffer is shown. The long-wavelength negative band is blue-shifted to 215 from 218 nm, and both the 215 and 195 nm bands have increased in intensity relative to the bands in the spectrum of the AcPHF6/HiPco SWCNT composite. The decrease in intensity in the spectrum of the composite relative that that of AcPHF6 in buffer is likely a result of a faction of the peptide bound to the CNTs resulting in a decrease in the effective solution concentration, while the red shift of the 215 nm band may reflect a slightly different environment on the CNT surface. The fact that no new CD bands appear in the spectrum of the composite compared to that of the peptide in buffer suggest that the HiPco SWCNTs make negligible contribution to the CD in this region, and no ellipticity was observed in the CD of HiPco SWCNTs suspended in SDS (Figure S1, Supporting Information).

The NIR spectra of peptide/HiPco SWCNT composites prepared with AcPHF6 and AcPHF6-related peptides having amino acid substitutions at the penultimate residue are shown in Figure 7A. All of the samples were prepared by sonication of the peptide (0.8 mM) and SWCNT sample in water followed by high speed centrifugation. There are general intensity differences between the spectra owing to differences in the ability of different peptides to disperse HiPco SWCNTs. We find that the two peptides that form negligible β-sheet containing amyloid in solution, AcVQIVAK and AcVQIVKK, also do not form composites with SWCNTs, having a low

dx.doi.org/10.1021/jp402057d | J. Phys. Chem. B 2013, 117, 7593−7604

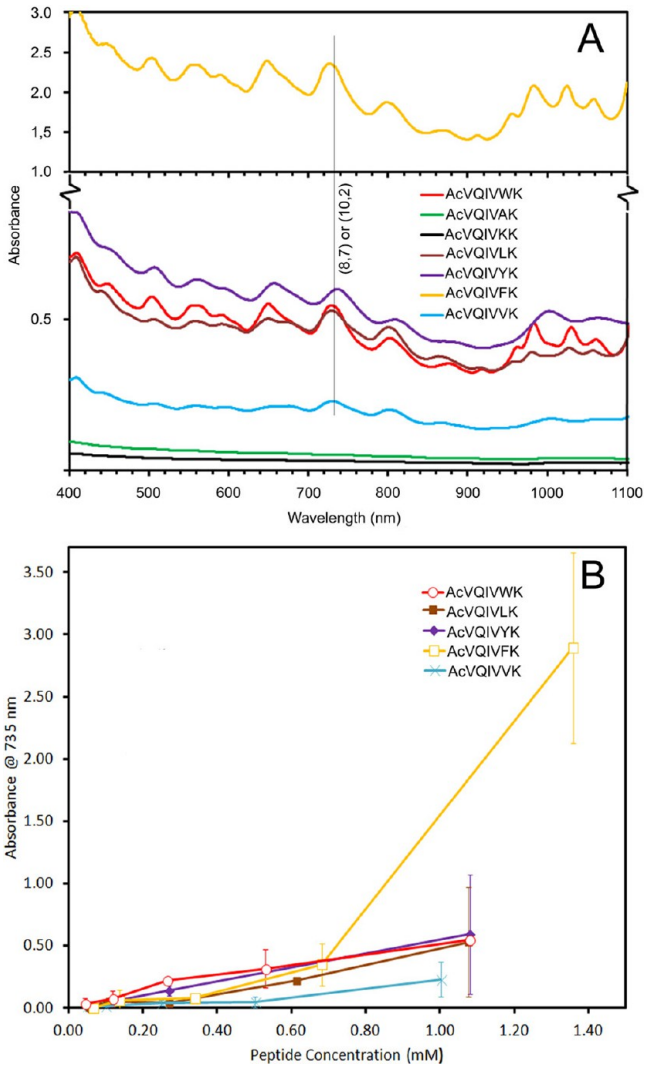

Figure 7. NIR spectra of HiPco SWCNT/AcVQIVXK composites prepared by sonicating HiPco SWCNTs in 1.0 (X = V), 1.08 (X = L, Y, W), or 1.36 mM (X = F) peptide (A). The (8,7) HiPco absorbance at 735 nm was used as a measure of the amount of SWCNTs dispersed (B).

relative absorbance over the entire spectral region. The remaining peptides that form amyloid appear to disperse SWCNTs but not necessarily in the order proportional to their amyloidogenic propensities[48] (Table 1). For example, AcPHF6 is calculated to have a higher amyloidogenic propensity than AcVQIVFK, but AcVQIVFK seems to disperse SWCNTs better based on its higher absorbance. We used the (8,7) SWCNT absorbance at 735 nm to quantitate these differences. Figure 7B shows that the amount of SWCNTs dispersed increases linearly with AcPHF6 concentration. In contrast, the same plot for AcVQIVFK is linear only up to 0.7 mM, above which the amount of SWCNTs dispersed increases dramatically. It is possible that this break in the curve represents a critical concentration above which higher-order peptide structures organize on the SWCNT surface. After AcVQIVFK, AcVQIVVK has the next highest amyloidogenic propensity but is only moderately effective at dispersing SWCNTs. In summary, our data indicate that factors other than a high propensity to form amyloid must be important in determining the ability of a peptide to disperse SWCNTs. Others have suggested that optimum optical properties were found using β-sheet-forming peptides that are imperfect assemblers in the absence of an external template such as a SWCNT.[26]

Differences between NIR spectra of the different peptide composites are also reflected in the fine structure that arises from van Hove transitions between the valence and conduction bands of semiconducting (E_{11}^S: 800−1600 nm; E_{22}^S: 500−900 nm) and metallic (E_{11}^M: 400−600 nm) SWCNTs.[1,14,15,26,29,30,57,74−76] Our assignments of these bands based on previous data for SWCNT composites with SDS, DNAs, and peptides are summarized in Table 2.[74−76]

All of the assignments in the NIR spectra (Table 2) arise from semiconducting tube types, while most of the bands in the RBM region of the Raman (with the exception of (7,5)) can be attributed to metallic tubes having van Hove singularities near to the 633 nm laser excitation. AcVQIVWK and AcVQIVLK seem to provide a higher degree of SWCNT debundling according to the better resolved vibronic structure observed in Figure 7A.[15,74−76] With respect to these, corresponding bands in the remaining amyloid forming peptides are broadened and red-shifted. For example, the bands at about 950 and 970 nm, which we have assigned to the E_{11} transitions of the (8,3) and (6,5) in SWCNT composites formed with AcVQIVLK and AcVQIVWK, are broadened and shifted to near 1000 nm in spectra of AcPHF6, AcVQIVVK, and AcVQIVFK composites. While many associate the narrow line width of van Hove transitions to debundling of SWCNTs,[1,14,15,29,30] it has been suggested that spatial nonuniformities in SWCNT coatings cause local variations in exciton binding energy that induce dephasing as the exciton moves along the nanotube axis. This alternative interpretation corresponds to variations in coating thickness observed for other self-assembling peptides/SWCNT composites.[26] The shift of bands to longer wavelength likely is the result of a more polar environment on the SWCNT surface.

As was pointed out previously, there is no clear correlation between the propensity of our peptides to self-assemble and their ability to disperse SWCNTs, as reflected by their NIR absorbance at 735 nm. We were interested in what other structural characteristics might account for this unique property. Figure 8A shows a bar plot of the (8,7) absorbance at 735 nm, the amyoidogenic propensity and hydrophobicity for peptides that were able to disperse SWCNTs. Peptides AcVQIVAK and AcVQIVKK were not included because they do not form composites with SWCNTs. We found by regression analysis that the NIR absorbance could be expressed as a linear combination of hydrophobicity and amyloidogenic propensity (normalized $C_1^2 = 0.59$; $C_2^2 = 0.41$; $R^2 = 0.996$) for peptides AcVQIVYK (AcPHF6), AcVQIVWK, AcVQIVLK, and AcVQIVVK (Figure 8B). The peptide AcVQIVFK had an unusually high absorbance and was an outlier from the linear trend. In summary, about 60% of the ability of four or the five peptides able to disperse SWCNTs can be attributed to hydrophobicity, while the other ~40% can be attributed to the ability of the peptides to form a β-sheet on the SWCNT surface.

Figure 9 compares the absorbance at 735 nm of SWCNTs sonicated with peptides AcYK, AcVYK, AcQIVYK, and AcPHF6. There is a clear dependence of length of these peptides on their ability to disperse SWCNTs. Although all of these peptides self-assemble to some extent to form amyloid,[46,48] the results suggest that longer peptides are better able to wrap around SWCNTs, forming a hydrogen-bonded β-sheet network. Similar results have been observed by others for

dx.doi.org/10.1021/jp402057d | J. Phys. Chem. B 2013, 117, 7593−7604

Table 2. Assignments for UV−Vis−NIR Absorption Bands for HiPco Composites with SDS or AcVQIVXK

L[b]	V	F	W	AcPHF6	HiPco/SDS	literature[c]	assignment[c]
408	409	409	410	409	410	407	(9,5) or (8,7)
441	441	445	448	445	447		
506	503	503	503	506	504	507	(7,3)
553	553	553	553	553	553	551	(6,5)
559			560			566	(9,2)
591	591	591	589	591	598	596	(8,4)
647	656	656	647	655	652	649	(7,5) or (7,6)
674						678	(9,5) or (8,3)
728	731	734	726	734	735	738	(8,7) or (10,2)
798	800	805	798	804	807	795	(10,5)
858	862	868	868	867	882		(6,4)
907			910			912	(9,1)
949			953		949	952	(8,3)
972			975		972	976	(6,5)
1022	1005[a]	1003[a]	1024	1001[a]	1015	1024	(7,5) or (7,3)
1048	1054	1054	1055	1054	1052	1053	(10,2)

[a]The assignment is unclear. These bands likely arise from a red-shifted and broadened E_{11} transition of (8,3) and (6,5) SWCNTs, which overlap with E_{11} transitions of (7,5) and (7,3) SWCNTs. [b]Peptide AcVQIVXK is abbreviated with a one letter code representative of residue "X". [c]Taken from refs 30, 57, and 74−76.

designed β-sheet peptides.[24,26] It has been suggested that the π-stacking interaction between aromatic amino acid side chains and the SWCNT surface and the amphiphilic character of a peptide can account for the ability of some peptides to disperse SWCNTs.[1,14−19,23,24,26−33] Should this be the case, one would expect that the zwitterionic form of aromatic amino acids might also be able to form composites with SWCNTs. Our data show this not to be the case for L-tyrosine or PHF6, further implying that the peptide backbone itself plays a crucial role in the interaction. In MOPS buffer, AcPHF6 readily self-assembles into amyloid filaments, and under these conditions, our results indicate that it has greater affinity for peptide−peptide interactions than for binding to and dispersing SWCNTs.

4. DISCUSSION

The interactions responsible for binding of polymers and biopolymers to SWCNTs depend not only on their chemical composition but also on their structural characteristics. Most macromolecules that are able to disperse SWCNTs in water are amphiphilic, with an aromatic or hydrophobic portion of the molecule attracted to the sp^2-hybidized surface of the CNT and a charged or polar portion pulling the combined nanotube/polymer complex into solution. In the case of peptides and some organic polymers, it has been argued that aromatic residues that promote $\pi-\pi$ stacking interactions between the polymer and the nanotube surface are important components of successful CNT dispersants.[1,14−19,23,24,28−33] However, one of the first and most successful dispersants, SDS, lacks such π-stacking interactions and relies upon encapsulation of SWCNTs in a micelle with hydrophobic tails interacting with the nanotube surface by van der Waals forces.[72] It is also interesting that poly-L-lysine, a polypeptide without aromatic side chains and little hydrophobic character, is able to disperse CNTs.[31,34] In this case, one can only assume that either the C_4H_8 in the lysine side chains or the peptide backbone interact favorably with the SWCNT surface, perhaps by van der Waals or a charge-transfer interaction.[15,30,37,38]

We refer to SDS as a vertical amphiphile because it has a charged head group and a long hydrophobic tail. Horizontal amphiphiles have been designed from peptides with alternating hydrophobic and hydrophilic residues alternating in the sequence. For these systems, the hydrophobic face of the peptide lies against the CNT surface, while the hydrophilic residues are turned outward toward the solvent.[1] It has long been known that horizontal amphiphilic peptides have a tendency to self-associate in solution, and it has been shown experimentally and in silico that these peptides wrap around SWCNTs in much the same manner as some organic polymers, polynucleic acids, and carbohydrates.[24,26,45] In the present study, we investigated the ability of a family of vertical amphiphilic peptides with predictable self-association characteristics (AcVQIVXK) to disperse SWCNTs. We found that the absorbance of these peptide/SWCNT composites in the NIR could not be explained by the amyloidogenic propensity alone. We used the HPLC retention time on a reverse phase column to approximate the hydrophobicity of these peptides and found that their ability to disperse SWCNTs could be explained by hydrophobicity and amyloidogenic propensity[48] (their propensity to form the β-sheet) in about a 60/40 ratio. The dependence of the absorbance of the dispersion as a function of peptide concentration revealed that the peptide AcVQIVFK had an unusually high ability to disperse SWCNTs, particularly at high peptide concentration. Given the particularly high affinity that tryptophan residues contained in other random coil peptides have for $\pi-\pi$ stacking interactions compared to other aromatic residues,[16,23] this result was surprising to us.

Our CD results suggest that in water, AcPHF6 exists as a random coil. When SWCNTs are sonicated in water containing the peptide, a dispersion is formed, and our CD results show that the peptide assumes a β-sheet structure. In MOPS buffer, the majority of the peptide exists in a fibrous amyloid state, as is reflected in the CD, and in this state, the peptide fails to disperse SWCNTs (Figure 9). These results suggest that the peptide first exists as a random coil and, following sonication with SWCNTs, begins to wrap the nanotubes, forming an extended β-sheet network. Our TEM and SEM results for AcPHF6 are consistent with the peptide coating of SWCNT bundles.[1] Raman spectra also suggest that AcPHF6 intercalates and coats SWCNT bundles and wrapping of SWCNTs. AcPHF6 peptides truncated at the N-terminal, including

dx.doi.org/10.1021/jp402057d | J. Phys. Chem. B 2013, 117, 7593−7604

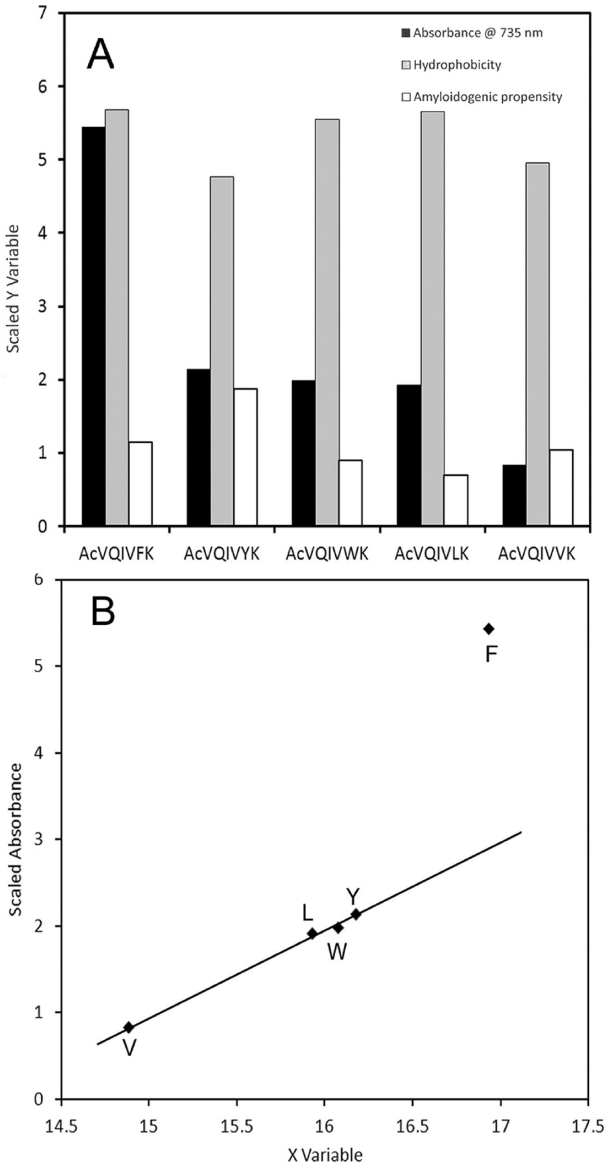

Figure 8. Absorbance at 735 nm of HiPco SWCNT/peptide composites; the peptide hydrophobicity is estimated from the HPLC retention time and amyloidogenic propensity[29] for selected peptides of general structure AcVQIVXK. All variables are scaled to unit variance (A). The absorbance could be fit to a linear combination of the scaled hydrophobicity and amyloidogenic propensity for peptides with X = L, W, Y, and V (B) (fitted coefficients for the hydrophobicity and propensity were 0.59 and 0.41 with r^2 = 0.996).

AcYK, AcVYK, and AcQIVYK, also form amyloid in the buffer, though at a reduced propensity compared to that of the parent peptide.[46] Due to their reduced propensity to form amyloid and their reduced hydrophobicity due to the elimination of the mostly hydrophobic tail, one might expect AcYK and AcVYK to be poorer dispersants of SWCNTs than AcPHF6, and this is indeed the case. The NIR absorbance of SWCNTs sonicated with these peptides is less than 1% of that seen for AcPHF6 (Figure 9). The zwitterionic form of AcPHF6, PHF6, also has a reduced hydrophobicity and amyloid-forming propensity and predictably is less efficient than AcPHF6 at dispersing SWCNTs. It was quite surprising, however, that the pentapeptide AcPHF5, which lacks only a terminal valine, was less than 10% as effective at dispersing SWCNTs as

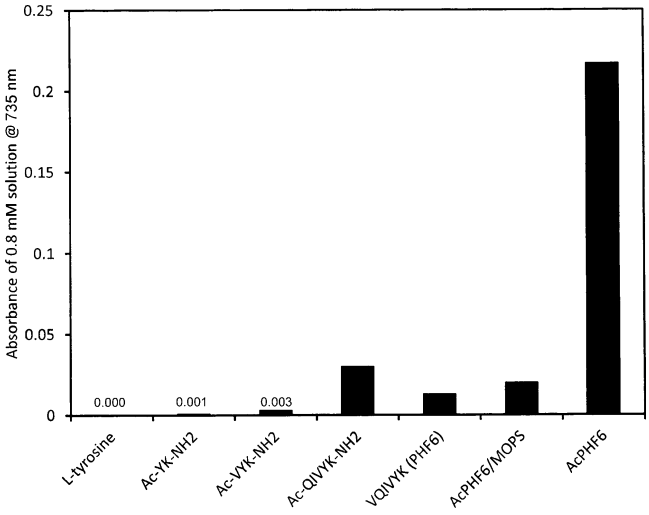

Figure 9. Absorbance at 735 nm of HiPco/amino acid or peptide composites. Samples were prepared by sonicating SWCNTs in water with 0.8 mM L-tyrosine or peptides AcYK, AcVYK, AcQIVYK, and VQIVYK (unblocked PHF6). Comparison is shown for the composites prepared from AcPHF6 in water and AcPHF6 in MOPS buffer.

AcPHF6. Because the hydrophobicity of this peptide was found to be quite near to that of the AcPHF6 (results not shown), it is likely that its reduced ability to form β-sheet structures profoundly influences its ability to bind to and disperse CNTs. Others have also shown that shortening of β-sheet peptides reduces their ability to disperse SWCNTs and attribute this to the reduced ability of the peptide to completely wrap the nanotube.[24,26,45]

5. CONCLUSION

We conclude from this study that β-sheet-forming peptides are able to noncovalently bind to and disperse SWCNTs. Peptides that give the best dispersions are those that (1) are a random coil in water but organize into a β-sheet network on the CNT surface, (2) are vertical or horizontal amphiphiles whereby hydrophobic residues interact with the SWCNTs by a combination of favorable interactions including $\pi-\pi$ stacking, van der Waals forces, and charge transfer and where charged or polar residues solvate the complex at the peptide−water interface, and (3) are of sufficient length to maximize favorable interactions and to wrap themselves around the nanotube.

The use of peptides to disperse CNTs has an advantage over other nonbiological polymers or amphiphiles in offering biocompatibility and over DNA-based systems in offering a minimally charged polymer. Many proteins[77,78] and peptides, selected by phage display[17,20−22,33] or designed de novo,[24−26] are seen to undergo a conformational change to a β-sheet upon binding to CNTs. Single amino acid substitutions in designed peptides have been observed to have profound effects on peptide−CNT binding,[24,26,29] and scrambling of the peptides sequence has been seen to destroy peptide interaction with CNTs altogether.[19] One may infer from these findings that the β-sheet conformation of peptides is energetically more favorable than other conformations for interacting with and solubilizing nanotubes and that the peptide−CNT interaction is highly dependent upon peptide sequence. Although α-helical peptides, charged on one face and hydrophobic on the other, have been shown to disperse CNTs,[1,7,15,29,30] these peptides are

dx.doi.org/10.1021/jp402057d | J. Phys. Chem. B 2013, 117, 7593−7604

quite long (29-mer), and β-sheet peptides designed de novo or selected by phage display are typically 12−16 residues.[17,20−22,33] To date, our hexapeptides based on the AcVQIVXK framework are structurally the simplest peptides that have been found to disperse CNTs. Furthermore, we have shown that the amyloidogenic propensity and hydrophobicity weigh nearly equally in determining their efficiency to disperse CNTs, and these findings may be used to design even more efficient peptides for these purposes. We believe that the structural simplicity of these peptides will have clear synthetic advantages over peptides now known to disperse CNTs.

■ ASSOCIATED CONTENT

Supporting Information

Far UV-CD spectra of HiPco SWCNT and a complete author list of cited references. This material is available free of charge via the Internet at http://pubs.acs.org.

■ AUTHOR INFORMATION

Corresponding Author

*E-mail: wgoux@utdallas.edu, phone: 972-883-2660, fax: 972-883-2925 (W.J.G.); E-mail: edgar@icb.csic.es, fax: 31-976-733318 (E.M.).

Notes

The authors declare no competing financial interest.

■ ACKNOWLEDGMENTS

This work has been supported by The University of Texas at Dallas, Robert A. Welch Grant AT-0029, and the regional Government of Aragón, Spain (Project PI119/09 and Research Groups funding). W.J.G. would like to thank Paul Pantano for lively discussions.

■ REFERENCES

(1) Dieckmann, G. R.; Dalton, A. B.; Johnson, P. A.; Razal, J.; Chen, J.; Giordano, G. M.; Muñoz, E.; Musselman, I. H.; Baughman, R. H.; Draper, R. K. Controlled Assembly of Carbon Nanotubes by Designed Amphiphilic Peptide Helices. *J. Am. Chem. Soc.* **2003**, *125*, 1770−1777.

(2) Nicolosi, V.; Cathcart, H.; Dalton, A. B.; Aherne, D.; Dieckmann, G. R.; Coleman, J. N. Spontaneous Exfoliation of Single-Walled Carbon Nanotubes Dispersed Using a Designed Amphiphilic Peptide. *Biomacromolecules* **2008**, *9*, 598−602.

(3) Yang, M.; Meng, J.; Mao, X.; Yang, Y.; Cheng, X.; Yuan, H.; Wang, C.; Xu, J. Carbon Nanotubes Induce Secondary Structure Changes of Bovine Albumin in Aqueous Phase. *Nanosci. Nanotechnol.* **2010**, *10*, 7550−7553.

(4) Baughman, R. H.; Zakhidov, A. A.; de Heer, W. A. Carbon Nanotubes — The Route Toward Applications. *Science* **2002**, *297*, 787−792.

(5) Guiseppi-Elie, A.; Lei, C.; Baughman, R. H. Direct Electron Transfer of Glucose Oxidase on Carbon Nanotubes. *Nanotechnology* **2002**, *13*, 559−564.

(6) Liu, Z.; Tabakman, S.; Welsher, K.; Dai, H. Carbon Nanotubes in Biology and Medicine: In Vitro and In Vivo Detection, Imaging and Drug Delivery. *Nano Res.* **2009**, *2*, 85−120.

(7) Chin, S. F.; Baughman, R. H.; Dalton, A. B.; Dieckmann, G. R.; Draper, R. K.; Mikoryak, C.; Musselman, I. H.; Poenitzsch, V. Z.; Xie, X.; Pantano, P. Amphiphilic Helical Peptide Enhances the Uptake of Single-Walled Carbon Nanotubes by Living Cells. *Exp. Biol. Med.* **2007**, *232*, 1236−1244.

(8) Marches, R.; Mikoryak, C.; Wang, R. H.; Pantano, P.; Draper, R. K.; Vitetta, E. S. The Importance of Cellular Internalization of Antibody-Targeted Carbon Nanotubes in the Photothermal Ablation of Breast Cancer Cells. *Nanotechnology* **2011**, *22*, 095101.

(9) Chakravarty, P.; Marches, R.; Zimmerman, N. S.; Swafford, A. D.; Bajaj, P.; Musselman, I. H.; Pantano, P.; Draper, R. K.; Vitetta, E. S. Thermal Ablation of Tumor Cells with Antibody-Functionalized Single-Walled Carbon Nanotubes. *Proc. Natl. Acad. Sci. U.S.A.* **2008**, *105*, 8697−702.

(10) in het Panhuis, M.; Gowrisanker, S.; Vanesko, D. J.; Mire, C. A.; Jin, H.; Xie, H.; Baughman, R. H.; Musselman, I. H.; Gnade, B. E.; Dieckmann, G. R.; et al. Nanotube Network Transistors from Peptide-Wrapped Single-Walled Carbon Nanotubes. *Small* **2005**, *1*, 820−823.

(11) Cui, Y.; Kim, S. N.; Naik, R. R.; McAlpine, M. C. Biomimetic Peptide Nanosensors. *Acc. Chem. Res.* **2012**, *45*, 696−704.

(12) Nunes, A.; Al-Jamal, K.; Nakajima, T.; Hariz, M.; Kostarelos, K. Application of Carbon Nanotubes in Neurology: Clinical Perspectives and Toxicological Risks. *Arch. Toxicol.* **2012**, *86*, 1009−1020.

(13) Paul, A.; Shao, W.; Shum-Tim, D.; Prakash, S. The Attenuation of Restenosis Following Arterial Gene Transfer Using Carbon Nanotube Coated Stent Incorporating TAT/DNA(Ang1+Vegf) Nanoparticles. *Biomaterials* **2012**, *33*, 7655−7664.

(14) Zorbas, V.; Ortiz-Acevedo, A.; Dalton, A. B.; Yoshida, M. M.; Dieckmann, G. R.; Draper, R. K.; Baughman, R. H.; Jose-Yacaman, M.; Musselman, I. H. Preparation and Characterization of Individual Peptide-Wrapped Single-Walled Carbon Nanotubes. *J. Am. Chem. Soc.* **2004**, *126*, 7222−7227.

(15) Poenitzsch, V. Z.; Winters, D. C.; Xie, H.; Dieckmann, G. R.; Dalton, A. B.; Musselman, I. H. Effect of Electron-Donating and Electron-Withdrawing Groups on Peptide/Single-Walled Carbon Nanotube Interactions. *J. Am. Chem. Soc.* **2007**, *129*, 14724−14732.

(16) Zheng, L.; Jain, D.; Burke, P. Nanotube−Peptide Interactions on Silicon Chip. *J. Phys. Chem. C* **2009**, *113*, 3978−3985.

(17) Deshpande, M. S.; Mazumdar, S. Sequence Specific Association of Tryptic Peptides with Multiwalled Carbon Nanotubes: Effect of Localization of Hydrophobic Residues. *Biomacromolecules* **2012**, *13*, 1410−1419.

(18) Wang, S.; Humphreys, E. S.; Chung, S.-Y.; Delduco, D. F.; Lustig, S. R.; Wang, H.; Parker, K. N.; Rizzo, N. W.; Subramoney, S.; Chiang, Y.-M.; et al. Peptides with Selective Affinity for Carbon Nanotubes. *Nat. Mater.* **2003**, *2*, 196−200.

(19) Kase, D.; Kulp, J. L., III; Yudasaka, M.; Evans, J. S.; Iijima, S.; Shiba, K. Affinity Selection of Peptide Phage Libraries Against Single-Wall Carbon Nanohorns Identifies a Peptide Aptamer with Conformational Variability. *Langmuir* **2004**, *20*, 8939−8941.

(20) Pender, M. J.; Sowards, L. A.; Hartgerink, J. D.; Stone, M. O.; Naik, R. R. Peptide-Mediated Formation of Single-Wall Carbon Nanotube Composites. *Nano Lett.* **2006**, *6*, 40−44.

(21) Witus, L. S.; Rocha, J.-D. R.; Yuwono, V. M.; Paramonov, S. E.; Weisman, R. B.; Hartgerink, J. D. Peptides that Non-Covalently Functionalize Single-Walled Carbon Nanotubes to Give Controlled Solubility Characteristics. *J. Mater. Chem.* **2007**, *17*, 1909−1915.

(22) Su, Z.; Leung, T.; Honek, J. F. Conformational Selectivity of Peptides for Single-Walled Carbon Nanotubes. *J. Phys. Chem. B* **2006**, *110*, 23623−23627.

(23) Su, Z.; Mui, K.; Daub, E.; Leung, T.; Nonek, J. Single-Walled Carbon Nanotube Binding Peptides: Probing Tryptophan's Importance by Unnatural Amino Acid Substitution. *J. Phys. Chem. B* **2007**, *111*, 14411−14416.

(24) Hashida, Y.; Umeyama, T.; Mihara, J.; Imahori, H.; Tsujimoto, M.; Isoda, S.; Takano, M.; Hashida, M. Development of a Novel Composite Material with Carbon Nanotubes Assisted by Self-Assembled Peptides Designed in Conjunction with β-Sheet Formation. *J. Pharm. Sci.* **2012**, *101*, 3398−3412.

(25) Jeong, W.; Lim, Y. Combination Self-Assembly of β-Sheet Peptides and Carbon Nanotubes: Functionalizing Carbon Nanotubes with Bioactive β-Sheet Block Copolypeptides. *Macromol. Biosci.* **2012**, *12*, 49−54.

(26) Tsyboulski, D. A.; Bakota, E. L.; Witus, L. S.; Rocha, J.-D.; Hartgerink, J. D.; Weisman, R. B. Self-Assembling Peptide Coatings Designed for Highly Luminescent Suspension of Single-Walled Carbon Nanotubes. *J. Am. Chem. Soc.* **2008**, *130*, 17134−17140.

(27) Sheikholeslam, M.; Pritzker, M.; Chen, P. Dispersion of Multiwalled Carbon Nanotubes in Water Using Ionic-Complementary Peptides. *Langmuir* **2012**, *28*, 12550−12556.
(28) Li, H.; Luo, Y.; Derreumaux, P.; Wei, G. Carbon Nanotube Inhibits the Formation of β-Sheet-Rich Oligomers of the Alzheimer's Amyloid-β(16−22) Peptide. *Biophys. J.* **2011**, *101*, 2267−2276.
(29) Xie, H.; Becraft, E. J.; Baughman, R. H.; Dalton, A. B.; Dieckmann, G. R. Ranking the Affinity of Aromatic Residues for Carbon Nanotubes by Using Designed Surfactant Peptides. *J. Pept. Sci.* **2008**, *14*, 139−151.
(30) Samarajeewa, D. R.; Dieckmann, G. R.; Nielsen, S. O.; Musselman, I. H. Modifying the Electronic Properties of Single-Walled Carbon Nanotubes Using the Designed Surfactant Peptides. *Nanoscale* **2012**, *4*, 4544−4554.
(31) Salzmann, C. G.; Ward, M. A. H.; Jacobs, R. M. J.; Tobias, G.; Green, M. L. H. Interaction of Tyrosine-, Tryptophan- and Lysine-Containing Polypeptides with Single-Wall Carbon Nanotubes and Its Televance for the Rational Design of Dispersing Agents. *J. Phys. Chem. C* **2007**, *111*, 18520−18524.
(32) Li, X.; Chen, W.; Zhan, Q.; Dai, L.; Sowards, L.; Pender, M.; Naik, R. R. Direct Measurements of Interactions Between Polypeptides and Carbon Nanotubes. *J. Phys. Chem. B* **2006**, *110*, 12621−12625.
(33) Kuang, Z.; Kim, S. N.; Crookes-Goodson, W. J.; Farmer, B. L.; Naik, R. R. Biomimetic Chemosensor: Designing Peptide Recognition Elements for Surface Functionalization of Carbon Nanotube Field Effect Transistors. *ACS Nano* **2010**, *4*, 452−458.
(34) Wang, D.; Chen, L. Temperature and pH-Responsive Single-Walled Carbon Nanotube Dispersions. *Nano Lett.* **2007**, *6*, 1480−1484.
(35) Dougherty, D. A. Cation−π Interactions in Chemistry and Biology: A New View of Benzene, Phe, Tyr, and Trp. *Science* **1996**, *271*, 163−167.
(36) Scrutton, N. S.; Raine, R. C. Cation−π Bonding and Amino−Aromatic Interactions in the Biomolecular Recognition of Substituted Ammonium Ligands. *Biochem. J.* **1996**, *319*, 1−8.
(37) Bradley, K.; Briman, M.; Star, A.; Grüner, G. Charge Transfer from Adsorbed Proteins. *Nano Lett.* **2004**, *4*, 253−256.
(38) Lin, Y.; Allard, L. F.; Sun, Y.-P. Protein-Affinity of Single-Walled Carbon Nanotubes in Water. *J. Phys. Chem. B* **2004**, *108*, 3760−3764.
(39) Zheng, M.; Jagota, A.; Semke, E. D.; Diner, B. A.; McLean, R. S.; Lustig, S. R.; Richardson, R. E.; Tassi, N. G. DNA-Assisted Dispersion and Separation of Carbon Nanotubes. *Nat. Mater.* **2003**, *2*, 338−342.
(40) Zheng, M.; Jagota, A.; Strano, M. S.; Santos, A. P.; Barone, P.; Chou, S. G.; Diner, B. A.; Dresselhaus, M. S.; McLean, R. S.; Onoa, G. B.; et al. Structure-Based Carbon Nanotube Sorting by Sequence-Dependent DNA Assembly. *Science* **2003**, *302*, 1545−1548.
(41) Hughes, M.; Cathcart, H.; Coleman, J. N. Dispersion and Exfoliation of Nanotubes with Synthetic Olionucleotides: Variation of Dispersion Efficiency and Oligo−Nanotube Interaction with Base Type. *J. Phys. Chem. C* **2010**, *114*, 11741−11747.
(42) Numata, N.; Asai, M.; Kaneko, K.; Hasegawa, T.; Fujita, N.; Kitada, Y.; Sakurai, K.; Shinkai, S. Curdlan and Schizophyllan (β-1,3-Glucans) Can Entrap Single-Wall Carbon Nanotubes in Their Helical Superstructure. *Chem. Lett.* **2004**, *33*, 232−233.
(43) Numata, M.; Sugikawa, K.; Kaneko, K.; Shinkai, S. Creation of Hierarchical Carbon Nanotube Assemblies Through Alternative Packing of Complementary Semi-Artificial β-1,3-Glucan/Carbon Nanotube Composites. *Chem.—Eur. J.* **2008**, *14*, 2398−2402.
(44) Ortiz-Acevedo, A.; Xie, H.; Zorbas, V.; Sampson, W. M.; Dalton, A. B.; Baughman, R. H.; Draper, R. K.; Musselman, I. H.; Dieckmann, G. R. Diameter-Selective Solubilisation of Single-Walled Xarbon Nanotubes by Reversible Cyclic Peptides. *J. Am. Chem. Soc.* **2005**, *127*, 9512−9517.
(45) Fu, Z.; Luo, Y.; Derreumaux, P.; Wei, G. Induced β-Barrel Formation of the Alzheimer's Aβ25−35 Oligomers on Carbon Nanotube Surfaces: Implication of Amyloid Fibril Inhibition. *Biophys. J.* **2009**, *97*, 1795−1803.
(46) Goux, W. J.; Kopplin, L.; Nguyen, A. D.; Leak, K.; Rutkofsky, M.; Shanmuganandam, V.; Sharma, D.; Inouye, H.; Kirschner, D. A. The Formation of Straight and Twisted Filaments from Short Tau Peptides. *J. Biol. Chem.* **2004**, *279*, 26868−26875.
(47) Inouye, H.; Sharma, D.; Goux, W. J.; Kirschner, D. A. Structure of Core Domain of Fibril-Forming PHF/Tau Fragments. *Biophys. J.* **2005**, *90*, 1774−1789.
(48) Rojas Quijano, F. A.; Morrow, D.; Wise, B. M.; Brancia, F. L.; Goux, W. J. Prediction of Nucleating Sequences from Amyloidogenic Propensities of Tau-Related Peptides. *Biochemistry* **2006**, *45*, 4638−4652.
(49) Moore, C. L.; Huang, M. H.; Robbennolt, S. A.; Voss, K. R.; Combs, B.; Gamblin, T. C.; Goux, W. J. Secondary Nucleating Sequences Affect Kinetics and Thermodynamics of Tau Aggregation. *Biochemistry* **2011**, *50*, 10876−10886.
(50) Zheng, J.; Liu, C.; Sawaya, M. R.; Vadla, B.; Khan, S.; Woods, J. R.; Eisenberg, D.; Goux, W. J.; Nowick, J. S. Macrocyclic β-Sheet Peptides that Inhibit the Aggregation of a Tau-Protein-Derived Hexapeptide. *J. Am. Chem. Soc.* **2011**, *133*, 3144−3157.
(51) Nikolaev, P.; Bronikowski, M. J.; Kelley Bradley, R.; Rohmund, F.; Colbert, D. T.; Smith, K. A.; Smalley, R. E. Gas-Phase Catalytic Growth of Single-Walled Carbon Nanotubes from Carbon Monoxide. *Chem. Phys. Lett.* **1999**, *313*, 91−97.
(52) Thess, A.; Lee, R.; Nikolaev, P.; Dai, H. J.; Petit, P.; Robert, J.; Xu, C. H.; Lee, Y. H.; Kim, S. G.; Rinzler, A. G.; et al. Crystalline Ropes of Metallic Carbon Nanotubes. *Science* **1996**, *273*, 483−487.
(53) Kosik, K. S.; Greenberg, S. M. Tau Protein and Alzheimer Disease. In *Alzheimer Disease*; Terry, R. D., Katzman, R., Bick, K. L., Eds.; Raven Press: New York, 1994; pp 335−344.
(54) von Bergen, M.; Friedhoff, P.; Biernat, J.; Heberle, J.; Mandelkow, E.-M.; Mandelkow, E. Assembly of τ Protein into Alzheimer Paired Helical Filaments Depends on a Local Sequence Motif (^{306}VQIVYK^{311}) Forming β Structure. *Proc. Natl. Acad. Sci. U.S.A.* **2000**, *97*, 5129−5134.
(55) Sawaya, M. R.; Sambashivan, S.; Nelson, R.; Ivanova, M. I.; Sievers, S. A.; Apostol, M. I.; Thompson, M. J.; Balbirnie, M.; Wiltzius, J. J. W.; McFarlane, H. T.; et al. Atomic Structures of Amyloid Cross-β Spines Reveal Varied Steric Zippers. *Nature* **2007**, *447*, 453−457.
(56) Dresselhaus, M. S.; Dresselhaus, G.; Saito, R.; Jorio, A. Raman Spectroscopy of Carbon Nanotubes. In *Carbon Nanotubes: Quantum Cylinders of Graphene*, Contemporary Concepts of Condensed Matter Science; Saito, S., Settl, A., Eds; Elsevier B.V.: Amsterdam, The Netherlands, 2008; Vol 3, pp 83−108.
(57) Bachilo, S. M.; Strano, M. S.; Kittrell, C.; Hauge, R. H.; Smalley, R. E.; Weisman, R. B. Structure-Assigned Optical Spectra of Single-Walled Carbon Nanotubes. *Science* **2002**, *298*, 2361−2365.
(58) Strano, M. S.; Zheng, M.; Jagota, A.; Onoa, G. B.; Heller, D. A.; Barone, P. W.; Usrey, M. L. Understanding the Nature of the DNA-Assisted Separation of Single-Walled Carbon Nanotubes Using Fluorescence and Raman Spectroscopy. *Nano Lett.* **2004**, *4*, 543−550.
(59) Strano, M. S.; Doorn, S. K.; Haroz, E. H.; Kittrell, C.; Hauge, R. H.; Smalley, R. E. Assignment of (*n*,*m*) Raman and Optical Features of Metallic Single-Walled Carbon Nanotubes. *Nano Lett.* **2003**, *3*, 1091−1096.
(60) Strano, M. S. Probing Chiral Selective Reactions Using a Revised Kataura Plot for the Interpretation of Single-Walled Carbon Nanotube Spectroscopy. *J. Am. Chem. Soc.* **2003**, *125*, 16148−16153.
(61) Hennrich, F.; Krupke, R.; Lebedkin, S.; Arnold, K.; Fischer, R.; Resasco, D. E.; Kappes, M. M. Raman Spectroscopy of Individual Single-Walled Carbon Nanotubes from Various Sources. *J. Phys. Chem. B* **2005**, *109*, 10567−10573.
(62) Kawamoto, H.; Uchida, T.; Kojima, K.; Tachibana, M. The Feature of the Breit−Wigner−Fano Raman Line in DNA-Wrapped Single-Wall Carbon Nanotubes. *J. Appl. Phys.* **2006**, *99*, 094309.
(63) Brown, S. D. M.; Jorio, A.; Corio, P.; Dresselhaus, M. S.; Dresselhaus, G.; Saito, R.; Kneipp, K. Origin of the Breit−Wigner−Fano Lineshape of the Tangential G-Band Feature of Metallic Carbon Nanotubes. *Phys. Rev. B* **2001**, *63*, 155414.

(64) Brown, S. D. M.; Corio, P.; Marucci, A.; Dresselhaus, M. S.; Pimenta, M. A.; Kneipp, K. Anti-Stokes Raman Spectra of Single-Walled Carbon Nanotubes. *Phys. Rev. B* **2000**, *61*, R5137.
(65) Heller, D. A.; Barone, P. W.; Swanson, J. P.; Mayrhofer, R. M.; Strano, M. S. Using Raman Spectroscopy to Elucidate the Aggregation State of Single-Walled Carbon Nanotubes. *J. Phys. Chem. B* **2004**, *108*, 6905−6909.
(66) Muñoz, E.; Suh, D.-S.; Collins, S.; Selvidge, M.; Dalton, A. B.; Kim, B. G.; Razal, J. M.; Ussery, G.; Rinzler, A. G.; Martínez, M. T.; et al. Highly Conducting Carbon Nanotube/Polyethyleneimine Composite Fibers. *Adv. Mater.* **2005**, *17*, 1064−1067.
(67) Dalton, A. B.; Stephan, C.; Coleman, J. N.; McCarthy, B.; Ajayan, P. M.; Lefrant, S.; Bernier, P.; Blau, W. J.; Byrne, H. J. Selective Interaction of a Semiconjugated Organic Polymer with Single-Wall Nanotubes. *J. Phys. Chem. B* **2000**, *104*, 10012−10016.
(68) Husanu, M.; Baibarac, M.; Baltog, I. Particular Signature of Isolated and Bundled Carbon Nanotubes in their Raman Spectra. *Rom. Rep. Phys.* **2008**, *60*, 691−699.
(69) Husanu, M.; Baibarac, M.; Preda, N.; Baltog, I. Resonant Raman Scattering and Absorption Spectroscopy Studies on Individual Carbon Nanotubes in Surfactant Solutions. *J. Optoelectron. Adv. Mater.* **2008**, *10*, 1722−1726.
(70) Rao, A. M.; Eklund, P. C.; Bandow, S.; Thess, A.; Smalley, R. E. Evidence for Charge Transfer in Doped Carbon Nanotube Bundles from Raman Scattering. *Nature* **1997**, *388*, 257−259.
(71) Woody, R. W. Theory of Circular Dichroism of Proteins. In *Circular Dichroism and the Conformational Analysis of Biomolecules*; Fasman, G. D., Ed.; Plenum Press: New York, 1996; pp 25−67.
(72) Woody, R. W. Aromatic Side-Chain Contributions to the Far Ultraviolet Circular Dichroism of Peptides and Proteins. *Biopolymers* **1978**, *17*, 1451−1467.
(73) Goux, W. J.; Hooker, T. M., Jr. Chiroptical Properties of Proteins. 1. Near-Ultraviolet Circular Dichroism of Ribonuclease S. *J. Am. Chem. Soc.* **1980**, *102*, 7080−7087.
(74) O'Connell, M. J.; Bachilo, S. M.; Huffman, C. B.; Moore, V. C.; Strano, M. S.; Haroz, E. H.; Rialon, K. L.; Bout, P. J.; Noon, W. H.; Kittrell, C.; et al. Band Gap Fluorescence from Individual Single-Walled Carbon Nanotubes. *Science* **2002**, *297*, 593−596.
(75) Tu, X.; Manohar, S.; Jagota, A.; Zheng, M. DNA Sequence Motifs for Structure-Specific Recognition and Separation of Carbon Nanotubes. *Nature* **2009**, *460*, 250−253.
(76) Weisman, R. B.; Bachilo, S. M. Dependence of Optical Transition Energies on Structure for Single-Walled Carbon Nanotubes in Aqueous Suspension: An Empirical Kataura Plot. *Nano Lett.* **2003**, *9*, 1235−1238.
(77) Azamian, B. R.; Davis, J. L.; Coleman, K. S.; Bagshaw, C. B.; Green, M. L. H. Bioectrocehmical Single-Walled Carbon Nanotubes. *J. Am. Chem. Soc.* **2002**, *124*, 12664−12665.
(78) Park, S. J.; Dongwoo, K. Conformational Changes of Fibrinogen in Dispersed Carbon Nanotubes. *Int. J. Nanomed.* **2012**, *7*, 4325−4333.